ЖЭТФ, 2014, том 146, вып. 6 (12), стр. 1282–1294

QUANTUM TRANSPORT EQUATION FOR SYSTEMS WITH ROUGH SURFACES AND ITS APPLICATION TO ULTRACOLD NEUTRONS IN A QUANTIZING GRAVITY FIELD

M. Escobar, A. E. Meyerovich*

Department of Physics, University of Rhode Island, Kingston RI 02881-0817, USA

Received May 7, 2014

We discuss transport of particles along random rough surfaces in quantum size effect conditions. As an intriguing application, we analyze gravitationally quantized ultracold neutrons in rough waveguides in conjunction with GRANIT experiments (ILL, Grenoble). We present a theoretical description of these experiments in the biased diffusion approximation for neutron mirrors with both one- and two-dimensional ($1D$ and $2D$) roughness. All system parameters collapse into a single constant which determines the depletion times for the gravitational quantum states and the exit neutron count. This constant is determined by a complicated integral of the correlation function (CF) of surface roughness. The reliable identification of this CF is always hindered by the presence of long fluctuation-driven correlation tails in finite-size samples. We report numerical experiments relevant for the identification of roughness of a new GRANIT waveguide and make predictions for ongoing experiments. We also propose a radically new design for the rough waveguide.

Contribution for the JETP special issue in honor of A. F. Andreev's 75th birthday

DOI: 10.7868/S0044451014120141

1. INTRODUCTION

The role of surface scattering increases dramatically with advances in micro- and nanofabrication, multilayer systems, pure materials, vacuum technology, etc. Below, we address some universal features of transport of particles or waves along random rough walls in quantum size effect conditions. As an application, we look at the gravitationally quantized ultracold neutrons in rough waveguides in conjunction with ongoing GRANIT experiments (ILL, Grenoble). This is one of the cleanest model-free testing grounds for our theory.

Intuitively, scattering by surface inhomogeneities should not be very different from scattering by other static defects such as bulk impurities. However, while the basic effects of impurity scattering are described in elementary textbooks, a similar simple general account for surface roughness has been missing. This is not entirely surprising. The underlying issue is an unusual structure of the perturbation theory. Randomly varying space inside corrugated systems makes it difficult to introduce a proper set of basis wave functions which are necessary for perturbative expansions. It is not always clear when this issue is important and what to do when it is.

Recently, we developed a consistent perturbative approach within which this issue disappears, clearing the way to a rigorous impurity-like description of quantum transport of particles in systems with rough boundaries. What is more, the structure of the corrugation-driven scattering probabilities is largely universal, irrespective of particle spectra, types of surfaces, and bulk fields between them.

The next section contains a simplified outline of our general transport results for systems with slight roughness, which are relevant for further discussion. In Sec. 3, we apply these results to beams of the gravitationally quantized neutrons in rough waveguides. In Sec. 4, we discuss correlation properties of random rough surfaces. We show that the identification of the roughness correlation function (CF) is not trivial and should not be based solely on a statistical quality of the fit to some fitting function. Section 5 contains our conclusions, experimental predictions, and recommendations.

*E-mail: Alexander_Meyerovich@uri.edu

2. QUANTUM SIZE EFFECT AND TRANSPORT OF PARTICLES ALONG RANDOMLY CORRUGATED WALLS

Theoretical approaches to particle transport in systems with random rough boundaries (see, e. g., books [1–4]; a brief review can be found in Ref. [5]) can be split into two main groups. The first one deals with boundary scattering by means of an effective boundary condition. We prefer alternative approaches that incorporate the boundary scattering directly into the bulk equations and allow using powerful bulk methods to describe the surface effects in transport and interference phenomena, localization, etc.

If we ignore potential complications, the simplest bulk-like approach [6] is a straightforward perturbation expansion in small corrugation $\xi(y,z)$ of the wall. We suppose that the wall is located at $x = x_\alpha + \xi_\alpha(y,z)$ and corresponds to an abrupt change of the potential by $[U]$,

$$U = [U]\,\theta\left(x - x_\alpha + \xi_\alpha(y,z)\right).$$

The small corrugation ξ_α looks like a good perturbation parameter,

$$U = [U]\,\theta(x - x_\alpha) + [U]\,\xi_\alpha\delta(x - x_\alpha) + \ldots$$

The calculation of the matrix element is trivial:

$$V_{ik}^{(\alpha)} = \int \exp\left(i\mathbf{s}\cdot(\mathbf{q}-\mathbf{q}')\right)\xi_\alpha(\mathbf{s})\,\Psi_i\Psi_k\,[U]\times \\ \times\,\delta(x - x_\alpha) = \xi(\mathbf{q}-\mathbf{q}')\,[U]\,\Psi_i(x_\alpha)\,\Psi_k(x_\alpha), \quad (1)$$

where $\Psi_i(x)$ are the wave functions in the absence of corrugation. This simple expression can be extended [5] to systems with rough external walls for which $[U]\to\infty$:

$$V_{ik}^{(\alpha)} = -\frac{1}{2m}\xi_\alpha(\mathbf{q}-\mathbf{q}')\,\Psi_i'(x_\alpha)\,\Psi_k'(x_\alpha). \quad (2)$$

If we need a more rigorous perturbative approach or want to study interference effects, a better option is to map the problem with the corrugated boundaries onto a mathematically equivalent problem with flat boundaries and distorted bulk [7–10]. Such mapping for a system with two rough walls,

$$x = \pm\frac{L}{2} \mp \xi_{1,2}(y,z), \quad (3)$$

can be achieved [9] by the coordinate transformation $\mathbf{r}\to\mathbf{R}$,

$$X = \frac{x + \xi_1/2 - \xi_2/2}{1 - \xi_1/L - \xi_2/L}, \quad Y = y, \quad Z = z, \quad (4)$$

which makes the boundaries straight, $X = \pm L/2$, without even specifying the single-valued random functions $\xi_{1,2}$. The rest is straightforward: we have to perform a conjugate transformation of momenta $\mathbf{p}\to\mathbf{P}$ and rewrite the original Hamiltonian $\widehat{H}_0(\mathbf{p},\mathbf{r})$ in terms of $\mathbf{R}$ and $\mathbf{P}$:

$$\widehat{H}_0(\mathbf{p},\mathbf{r}) = \widehat{H}_0(\mathbf{P},\mathbf{R}) + \widehat{V}\left(\mathbf{P},\mathbf{R},\{\xi_{1,2}(\mathbf{R})\}\right). \quad (5)$$

The result is the exactly equivalent problem in which the (random) bulk perturbation operator $\widehat{V}$ replaces the surface inhomogeneities. In simple situations, the matrix elements of $\widehat{V}$ are similar to (1) and (2). The drawback of mapping transformation (4) is that its Jacobian $J \neq 1$. When this is important, the transformation can be modified [10].

The diagrammatic derivation of the transport equation for systems with random surface inhomogeneities has been done in Ref. [10]. The restricted motion perpendicular to the walls is quantized, $(p_x)_j \sim j\hbar/L$, $E(\mathbf{p}) \to E_j(\mathbf{q})$, where $\mathbf{q} = (p_y, p_z)$ is the two-dimensional momentum. This quantization is important for ultrathin systems, multilayer media, interconnects, particles absorbed on or bound to the surfaces, quantum wells, etc. The transport equation is quantum in the direction perpendicular to the walls and is quasiclassical along the walls. In ultrathin systems with a large separation between the minibands E_j, as well as in thick quasiclassical films, the transport equation has a usual Boltzmann-like form,

$$\partial_t\delta n_j(\mathbf{q}) + \frac{\mathbf{q}}{m}\cdot\partial_{\mathbf{r}}\delta n_j(\mathbf{q}) + \mathbf{F}\cdot\partial_{\mathbf{q}}\delta n_j(\mathbf{q}) = \\ = L_j\{n_i\}. \quad (6)$$

In-between, there is an anomalous regime in which the transport equation acquires a highly unusual and complicated form [10]; we do not deal with this situation here. Since the mapping transformation approach is mathematically rigorous, it can be extended to more complex situations, including the surface-driven localization [11], interference between surface and bulk scattering processes [12], topological phase transitions [13], etc.

The perturbative collision integrals L_j are determined by the transition probabilities $W_{jj'}(\mathbf{q},\mathbf{q}') = \left\langle |V_{j\mathbf{q},j'\mathbf{q}'}|^2 \right\rangle$ between the states $(j,\mathbf{q})\to(j',\mathbf{q}')$:

$$L_j = 2\pi\sum_{j'}\int W_{jj'}(\mathbf{q},\mathbf{q}')\,[n_{j'\mathbf{q}'} - n_{j\mathbf{q}}]\times \\ \times\,\delta(\epsilon_{j\mathbf{q}} - \epsilon_{j'\mathbf{q}'})\,\frac{d^2q'}{(2\pi\hbar)^2}. \quad (7)$$

Generally, the transition probabilities $W_{jj'}(\mathbf{q},\mathbf{q}')$ factor into the products of the CF of surface roughness $\zeta(\mathbf{q}-\mathbf{q}')$ and the boundary values of the wave functions Ψ_j in the absence of corrugation. These combinations depend on the structure of the system, the number of interfaces, and the correlation between inhomogeneities from different walls.

The CF of surface inhomogeneities $\zeta_{\alpha\beta}(|\mathbf{s}|)$ and its power spectrum $\zeta_{\alpha\beta}(|\mathbf{q}|)$ are defined as

$$\begin{aligned}\zeta_{\alpha\beta}(|\mathbf{s}|) &= \langle\xi_\alpha(\mathbf{s}_1)\xi_\beta(\mathbf{s}_1+\mathbf{s})\rangle \equiv \\ &\equiv A^{-1}\int \xi_\alpha(\mathbf{s}_1)\xi_\beta(\mathbf{s}_1+\mathbf{s})\,d\mathbf{s}_1, \\ \zeta_{\alpha\beta}(|\mathbf{q}|) &= \int d^2s\exp\left(\frac{i\mathbf{q}\cdot\mathbf{s}}{\hbar}\right)\zeta_{\alpha\beta}(|\mathbf{s}|) = \\ &= 2\pi\int\limits_0^\infty \zeta_{\alpha\beta}(s)\,J_0(qs)\,s\,ds,\end{aligned} \tag{8}$$

where A is the area, and the indices α,β indicate the surfaces that are the sources of inhomogeneities ξ_α and ξ_β.

If the system has only one rough surface at $x = L+\xi(y,z)$ with the potential jump $[U]$ on it, then, according to Eq. (1),

$$W_{jj'} = \zeta(\mathbf{q}-\mathbf{q}')\,[U]^2\,|\Psi_j(L)|^2\,|\Psi_{j'}(L)|^2. \tag{9}$$

If, on the other hand, there are several interfaces at $x_\alpha = L_\alpha+\xi_\alpha(y,z)$ with different discontinuities $[U]_\alpha$, then

$$\begin{aligned}&W^{\alpha\beta}_{jj'} = \\ &= \mathrm{Re}\left[\zeta_{\alpha\beta}(\mathbf{q}-\mathbf{q}')\,[U]_\alpha\,[U^*]_\beta\,\Psi^*_{j\alpha}\Psi_{j'\alpha}\Psi_{j\beta}\Psi^*_{j'\beta}\right],\end{aligned} \tag{10}$$

where $\Psi_\alpha = \Psi(L_\alpha)$. The full scattering probability W is the sum of all these $W^{\alpha\beta}$. For a system with two external walls with $[U]_{1,2}\to\infty$, Eq. (2), the probabilities W are

$$W^{\alpha\beta}_{jj'} = \frac{1}{4m^2}\,\mathrm{Re}\left[\zeta_{\alpha\beta}\Psi^{*\prime}_{j\alpha}\Psi'_{j'\alpha}\Psi'_{j\beta}\Psi^{*\prime}_{j'\beta}\right], \qquad \alpha,\beta=1,2 \tag{11}$$

and the interference between inhomogeneities on the external wall (α) and the internal interface (β) yields

$$W^{\alpha\beta}_{jj'} = \frac{-1}{2m}\,\mathrm{Re}\left[\zeta_{\alpha\beta}U_\beta\Psi^{*\prime}_{j\alpha}\Psi'_{j'\alpha}\Psi_{j\beta}\Psi^*_{j'\beta}\right]. \tag{12}$$

Equation (10) for internal interfaces is the same irrespective of the particle spectrum, while Eqs. (11) and (12) are given for $\epsilon = p^2/2m$ (equations for arbitrary $\epsilon(\mathbf{p})$ are more cumbersome [5]).

The terms with $\alpha=\beta$ and $\alpha\neq\beta$ describe the intrawall and interwall correlations of inhomogeneities. The interwall contribution $\alpha\neq\beta$, when it exists [14], is nontrivial. While $W^{\alpha\alpha}$ is always positive, the sign of the interwall term $W^{\alpha\beta}$ with $\alpha\neq\beta$ is not fixed, and the interwall interference can be constructive or destructive depending on a particular realization of the system (overall, W is positive because $\zeta_{\alpha\alpha}(\mathbf{q})+\zeta_{\beta\beta}(\mathbf{q}) > 2|\zeta_{\alpha\beta}(\mathbf{q})|$ for any corrugation). For illustration, here is the full roughness-driven transition probability for particles with the quadratic spectrum in a homogeneous quantum well with infinite potential walls:

$$W_{jj'} = \frac{1}{m^2L^2}\left[\zeta_{11}+\zeta_{22}+2(-1)^{j+j'}\zeta_{12}\right]\times \\ \times\left(\frac{\pi j}{L}\right)^2\left(\frac{\pi j'}{L}\right)^2. \tag{13}$$

The interwall correlation term with ζ_{12} has an oscillating structure and can sometimes lead to a large increase in transport coefficients [15].

The collision operator and transition probabilities (7)–(13) have a simple structure and, with the exception of the interference terms, resemble those for impurity scattering with the roughness CF ζ playing the role of the impurity scattering cross section σ_{imp}. Therefore, transport calculations could be done essentially in the same way as for bulk impurities. The quantization of motion actually simplifies the problem by replacing the integral transport equation by a finite set of coupled linear equations. Under certain conditions, these equations decouple and we can obtain semi-analytic results for the transport coefficients via the zeroth and first harmonics of the roughness CF [5, 15, 16].

3. APPLICATION TO GRAVITATIONALLY QUANTIZED ULTRACOLD NEUTRONS IN ROUGH WAVEGUIDES

Recent observation by the GRANIT group (ILL, Grenoble) [17] of quantization of motion of ultracold neutrons by Earth's gravitational field predicted in Ref. [18] is an exciting breakthrough in neutron physics (see also reviews [19] and Refs. [20, 21]; for general properties of ultracold neutrons, see Refs. [22]). Although the quantization of motion by a linear field such as gravity is not new by itself [23] and has already been observed in a low-temperature context [24], the experimental access to well-defined neutron states in the 1 peV range opens the way for using ultracold neutrons as a very sensitive probe for extremely weak fundamental forces [19, 25, 26].

The experiment is based on sending a beam of ultracold neutrons between two horizontal mirrors. The top mirror is intentionally made rough, while the flat bottom one can ensure thousands of consecutive specular reflections [27] if the vertical velocity of neutrons is below a certain threshold (about 4 m/s in GRANIT experiments). If the vertical velocity exceeds this threshold, the neutrons penetrate the mirrors and disappear. The ultracold neutrons entering the waveguide have a large horizontal velocity comparable to the penetration threshold, and, as a result of collimation, a much smaller residual vertical velocity. The scattering of neutrons by the rough upper mirror turns the velocity vector and increases its vertical component, leading to an eventual escape of neutrons through the mirrors. The quantization of the vertical motion of neutrons by Earth's gravity field discretizes the amplitudes of bounces of neutrons from the bottom mirror. The roughness-driven turning of the velocity corresponds to the scattering-driven transitions of neutrons into higher quantum states j. Only the neutrons in the lowest gravitational states, which have the lowest amplitudes of bounces, cannot reach the rough upper mirror and continue bouncing along the bottom mirror until they reach the exit neutron counter. In principle, decreasing the separation between the mirrors should result in a stepwise disappearance of neutrons from lower and lower states. So far, this stepwise depletion of the gravitational quantum states has not been observed. The question is, why?

Earlier [28, 29], we developed a theoretical framework for describing experiments with collimated beams of ultracold neutrons in rough waveguides and demonstrated that the neutron count depends on the correlation properties of the rough mirror [30]. The agreement between our theory and experiment was actually better than one would expect with the uncertainty in the input parameters existing at the time. An alternative description of the same experiment [31] used a large set of independent fitting parameters that were unrelated to the properties of the waveguide.

Below, we finalize our theory with an eye on the ongoing experiments with a new waveguide. Among other things, we include scattering in all, and not only vertical, directions, derive scaling equations for the depletion times and the exit neutron count, and develop methods for identification of the roughness CF in application to the experimental data for the new rough mirror. We also demonstrate that the fitting parameters used in Ref. [31] as independent have universal ratios.

We use dimensionless variables, which are common to the field (for details, see Ref. [29]). All distances z are measured in units of l_0, $s = z/l_0$, where $l_0 = \hbar^{2/3}\left(2m^2g\right)^{-1/3} \approx 5.871$ μm is the size of the lowest quantum state in the infinite gravitational trap (open geometry without the upper mirror). The dimensionless distance between the mirrors $h = H/l_0$ in experiment typically does not go below 2. The main parameters of the roughness CF, namely, the average amplitude and the correlation radius of surface roughness $\eta = \ell/l_0$ and $r = R/l_0$, are usually within the 0.1–1 range. The energies are measured in units of e_0, where $e_0 = mgl_0 \approx 0.602$ peV$\approx 9.6366 \cdot 10^{-32}$ J is the energy of a neutron in the lowest quantum state. The lowest quantized levels in the gravity field $\lambda_j = \epsilon_j/e_0$ are below 10 while the typical overall kinetic energy of particles in the beam $\varepsilon = E/e_0$ and the absorption threshold $u_c = U_c/e_0$ are of the order of 10^5. Thus, the details of the potential near the absorption threshold are irrelevant for the lowest gravitational states $\lambda_j \ll u_c, \varepsilon$. The energy spectrum $\lambda_j(h)$ and the wave functions Ψ_j can be found in Refs. [28, 29]. In the original GRANIT cell, $\chi \equiv u_c/\varepsilon \approx 0.16$, and in a new one, $\chi \approx 1$. The horizontal velocities v_j (momenta q_j) in the beam direction are measured in units of

$$v_0 = \sqrt{2gl_0} = \frac{\hbar}{ml_0} \approx 1.073 \cdot 10^{-2} \text{ m/s},$$

$$\beta_j = \frac{v_j}{v_0} = \sqrt{\varepsilon - \lambda_j} \equiv \frac{q_j l_0}{\hbar}.$$

The scale for characteristic times is provided by the oscillation frequency of neutrons in the gravitational well,

$$\frac{1}{\tau_0} = \frac{\sqrt{2\pi}}{4m}\frac{\hbar}{l_0^2} \approx 1148.7 \text{ s}^{-1}. \tag{14}$$

The time of flight of neutrons through the old cell [17] is $t_L/\tau_0 \approx 23$. In the new cell [32], $t_L/\tau_0 \approx 26$.

Time evolution of the occupancy of the gravitational states $n_j(\mathbf{q})$ is governed by transport equation (6), (7):

$$\partial_t n_j(\mathbf{q}) = 2\pi \sum_{j'} \int \frac{d^2q'}{(2\pi\hbar)^2} \left[W_{jj'}(|\mathbf{q}-\mathbf{q}'|)\, n_{j'\mathbf{q}'} - \right.$$

$$\left. - W_{jj'}(|\mathbf{q}-\mathbf{q}'|)\, n_{j\mathbf{q}}\right] \delta\left(\epsilon_j - \epsilon_{j'} + \frac{q^2 - q'^2}{2m}\right), \tag{15}$$

with transition probabilities $W_{jj'}(|\mathbf{q}-\mathbf{q}'|)$ given either by Eq. (9) with $[U] = U_c$ or Eq. (11). The contribution from the direct transitions to the states above the absorption threshold U_c is negligible [29]. Integration

with the energy δ-function in the relaxation time approximation $n_j(\mathbf{q}) = \delta(q - q_j) N_j$ reduces Eqs. (15) to

$$\partial_t N_j = \frac{m}{2\pi} \sum_{j'} \int d\theta \left[W_{jj'} \left(\left| \mathbf{q}_j - \mathbf{q}_{j'} \right| \right) N_{j'} - \right.$$
$$\left. - W_{jj'} \left(\left| \mathbf{q}_j - \mathbf{q}_{j'} \right| \right) N_j \right], \quad (16)$$

where $q_j^2/2m = E - \epsilon_j$ and θ is the angle between $\mathbf{q}_j$ and $\mathbf{q}_{j'}$.

The diffusion of neutrons between the quantum states j has a strong directional bias upward, towards higher j [29]. The bias is explained by the rapid growth of the product of wave functions in Eqs. (9) and (11) with increasing j and j' (roughly, as $j^2 j'^2$, see Eqs. (13)). This increase in the rate of jumps $j \to j'$ is reversed by the rapid decay of the CF $\zeta\left(\left|\mathbf{q}_j - \mathbf{q}_{j'}\right|\right)$ at large $\left|\mathbf{q}_j - \mathbf{q}_{j'}\right| \gtrsim 1/R$. As a result, as a function of j', the transition rates $j \to j'$ represent a relatively narrow peak around some $j_1 \gg j$. This upward bias is so strong that almost all the time τ_j necessary for a neutron from a low gravitational state j to go up in states and disappear over the absorption barrier U_c, is spent on the first transition upwards.

This strong upward bias allows neglecting the transitions from the higher states down in transport equation (16) for the lowest states:

$$\partial_t N_j = -\frac{N_j}{\tau_j},$$
$$\frac{1}{\tau_j} = m \sum_{j'} \int \frac{d\theta}{2\pi} W_{jj'} \left(\left| \mathbf{q}_j - \mathbf{q}_{j'} \right| \right), \quad (17)$$

while the depletion times τ_j for the lowest gravitational states j differ from each other, according to Eq. (9), only by the values of the wave functions on the rough mirror $\Psi_j^2(H)$,

$$\frac{1}{\tau_j} = \frac{b_j}{b_1} \frac{1}{\tau_1}, \quad b_j = \frac{10^5 l_0 \Psi_j^2(H)}{2}, \quad (18)$$

where τ_1 is the depletion time for neutrons in the lowest gravitational state (these depletion times are used as independent fitting parameters in Ref. [31]). The ratios $\tau_j(h)/\tau_1(h)$, Eq. (18), are plotted in Fig. 1 for $j = 2, 3, 4, 5$ as a function of the slit width h. These ratios, which measure the relative widths of the eigenstates in the biased diffusion approximation, are the same for one-dimensional ($1D$) and two-dimensional ($2D$) roughness and do not depend on the roughness parameters at all (the $1D$ roughness is a random grating perpendicular to the beam direction). The stepwise dependence of the exit neutron count N_e on h can be observed only if the values of $t_L/\tau_j = (t_L/\tau_1)(b_j/b_1)$ are not too close to each other.

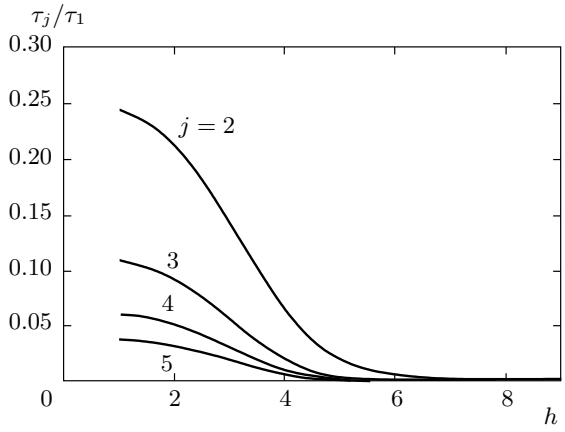

Fig. 1. The ratios $\tau_j(h)/\tau_1(h)$, Eq. (18), for the lowest quantum levels $j = 2, 3, 4, 5$ as functions of the slit width h. The curves are marked by the values of j. These functions are the same for $1D$ and $2D$ roughness and do not depend on the roughness parameters

The values of $\tau_j(h)$ determine the depletion of each quantum state j and the overall exit neutron count N_e,

$$N_e = \sum N_j = \sum N_j(0) \exp(-L/v_j \tau_j), \quad (19)$$

where $N_j(0)$ is the number of neutrons in a state j entering the waveguide of the length L. Equation (18) shows that for the lowest levels with $v_j \approx \sqrt{\varepsilon} v_0$, all relevant parameters collapse into a single constant Φ,

$$N_e = \sum N_j(0) \exp(-\Phi b_j(h)), \quad (20)$$

$$\Phi(h) = L/v_0 \tau_1 b_1(h), \quad (21)$$

and the only remaining task is to calculate τ_1 (or Φ). The time τ_1 strongly depends on roughness, making Φ different for $1D$ and $2D$ roughness, $\Phi_1 \neq \Phi_2$.

In the biased diffusion approximation, transport equations (15) decouple and

$$\frac{\tau_0}{\tau_1} = 2 \cdot 10^{-5} b_1 u_c^2 \gamma^2 F_2(r, h), \quad (22)$$

$$F_2(r, h) = 10^{-5} \sqrt{\frac{2}{\pi}} r^4 \sum_{\lambda_j < u_c/\chi} b_j(h) \psi_2(y_1, y_j), \quad (23)$$

$$y_1 = r\sqrt{\frac{u_c}{\chi}}, \quad y_j = q_j r = r\sqrt{\frac{u_c}{\chi} - \lambda_j}, \quad (24)$$

where $\psi_2(y_j, y_{j'})$ is the dimensionless zeroth harmonic of the CF $\zeta(|\mathbf{q}_j - \mathbf{q}_{j'}|)$ over the angle between the vectors $\mathbf{q}_j$ and $\mathbf{q}_{j'}$,

$$\psi_2(y_j, y_{j'}) = \zeta^{(0)}(q_j, q_{j'})/\ell^2 R^2.$$

The subscript "2" in F_2, ψ_2 points at $2D$ roughness. The main contribution to the sum in Eq. (23) comes from the terms with large j, and we can replace it by the integral,

$$F_2(r,h) = r^4\sqrt{\frac{2u_c}{\pi^3\chi^3}}\int\limits_0^1 z^2\psi_2(y_1,\widetilde{y})\,dz, \tag{25}$$

where $y_1 = r\sqrt{u_c/\chi}$ and $y_j \to \widetilde{y} = r\sqrt{1-z^2}\sqrt{u_c/\chi}$. If all initial occupancies are the same, $N_j(0) = N_0$, then N_e in Eq. (20) becomes

$$N_e = N_0 f(r,h) = N_0\sum \exp\left(-\Phi_2 b_j(h)\right), \tag{26}$$

$$\Phi_2(\eta,r) = A_2\eta^2 r^2\int\limits_0^1 z^2\psi_2(y_1,\widetilde{y})\,dz, \tag{27}$$

$$A_2 = \left(\frac{2}{\pi}\right)^{3/2}\cdot 10^{-5}\frac{t_L}{\tau_0}\frac{u_c^{5/2}}{\chi^{3/2}}. \tag{28}$$

The equation for the exit neutron count N_e for the waveguide with $1D$ roughness (grating) is the same as Eq. (26), but with Φ_1 instead of Φ_2 [30]:

$$\begin{aligned}\Phi_1(\eta,r) &= A_1\eta^2 r\int\limits_0^1 z^2\psi_1(y)\,dz,\\ y &= \sqrt{u_c/\chi}\,r\left(1-\sqrt{1-z^2}\right),\\ A_1 &= 4\cdot 10^{-5}t_L u_c^2/\tau_0\pi\chi.\end{aligned} \tag{29}$$

The calculation of the exit neutron count (26) reduces to the integration of the CF for the rough mirror. The result strongly depends on the shape of the CF. There are no experimental data on the roughness CF of the original mirror. The only information is that the typical lateral and vertical sizes of inhomogeneities are about $1.19\ell_0$ and $0.119\ell_0$. In the absence of the data, it was assumed in Ref. [30] that the roughness is $1D$ Gaussian with $r = 1.19$ and $\eta = 0.119$. At the end of next section, we analyze the roughness of the new mirror. Our prediction for the neutron count (26) for this new mirror is given in Sec. 5.

It is possible to perform analytic integrations in Eq. (29) for most common types of $1D$ CFs. For example, the exponential CF $\zeta(x) = \eta^2\exp(-x/r)$ yields

$$\Phi_1 \approx \frac{1}{3}A_1\eta^2 r\,{}_2F_1\left(\frac{3}{4},\frac{3}{2},\frac{7}{4},-\frac{r^2u_c}{4\chi}\right) \approx \approx 1.38\frac{A_1\eta^2}{r^{1/2}}\frac{(4\chi)^{3/4}}{3u_c^{3/4}}. \tag{30}$$

In the $2D$ case, the expressions for the zeroth angular harmonics for the power spectrum $\zeta^{(0)}(|\mathbf{q}-\mathbf{q}'|)$ are too complicated even for the simplest CFs [16] and the integration in Eq. (27) is done numerically.

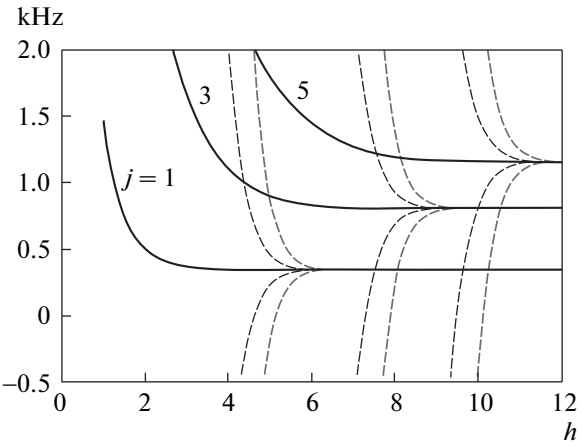

Fig. 2. The energies of the gravitational quantum states $\epsilon_j(h)$ for $j = 1, 3, 5$ as functions of the waveguide width h (solid lines). The dashed lines show the line broadening $\epsilon_j \pm 1/2\tau_j$ in kHz. The roughness is exponential in one (black dashed lines) or two (grey dashed lines) dimensions with $\eta = r = 1$. Scaling (31) allows recalculating the broadening for different η and r

For moderate values of $r > 0.3$, the depletion times τ_j and the parameter Φ scale as

$$1/\tau_j, \Phi = C_{\tau,\Phi}\eta^2 r^\gamma, \tag{31}$$

where the coefficients $C_{\tau,\Phi}$ depend on the dimensionality and the shape of the CF, Eqs. (27) and (29). At $u_c \to \infty$, the scaling index $\gamma = -1/2$ in both $1D$ and $2D$. If $u_c \sim 10^5$, as in experiment, the scaling index for exponential roughness is $\gamma \approx -0.465$ in $2D$ and $\gamma \approx -0.494$ in $1D$ (cf. Eq. (30)).

The times $\tau_j(h)$ describe the depletion and broadening of the quantum gravitational states, $\epsilon_j(h) \to \epsilon_j(h) + i\hbar/\tau_j(h)$. In Fig. 2, we plot $\epsilon_j(h)$ for $j = 1, 3, 5$ as a function of the waveguide width h (solid black lines) together with the line broadening $\epsilon_j \pm \hbar/2\tau_j$ (dashed lines) in kHz. The roughness is exponential in $1D$ (black dashed lines) or $2D$ (grey dashed lines) with $\eta = r = 1$. Equation (31) allows rescaling of the line broadening for other values of η and r. The individual quantum states become meaningless when the line broadening becomes comparable to the separation between the lines. The simplest way to preserve the states is to decrease the roughness amplitude η in comparison to its value $\eta = 1$ in Fig. 2.

These values of the line broadening/depletion times, in combination with our predictions for the exit neutron

count $N_e(h)$, Eq. (26), provide the full description of the problem (see Sec. 5). The quantum steps in $N_e(h)$ become pronounced with an increase in $\eta^2/r^{1/2}$ and the time of flight t_L. The only remaining issue is the value of the correlation parameters.

4. CORRELATION PROPERTIES OF ROUGH SURFACES

Practical applications of the transport theory require the CF of surface inhomogeneities as an input. Often, various Gaussian, exponential, and power-law functions are chosen at will in lieu of an unknown CF without giving it a second thought. It is routinely assumed that if one needs the accurate CF, one could always extract it from STM, AFM, and other precise measurements of surface profiles (some requirements for profile measurements are discussed, e. g., in Refs. [33, 34]).

The profile measurement provides one with a big data set of discrete correlation parameters. The next steps look straightforward: one could either identify the CF using reasonable fitting functions or input these raw correlation parameters directly into the equations. But how reliable are these choices?

The best way to test this is to study rough surfaces with the known roughness correlators. This is hardly feasible: the roughness correlators depend on the surface preparation and are not known beforehand. The best alternative is to computationally generate surfaces with predetermined correlators, "measure" their profiles, extract the correlators, and compare them to the "true" CF used to generate the surface. Below, we report the results of such numerical experiments (for technical details and broader applications, see Ref. [35]).

The CFs extracted from our numerical experiments have been fitted to Gaussian, exponential, and power-law functions or used directly in transport computations including $\Phi_{1,2}$ for our neutron problem. The purpose is to see how sensitive the results for $\Phi_{1,2}$ (the depletion times and the exit neutron count) are to a choice of the fitting function and, by extension, how we should use the correlation data sets extracted from the real experimental data. We apply these conclusions at the end of this section to the experimental data for the new neutron mirror.

We start from a discretized random rough profile $\mathbf{g} = g(x_i)$ generated using a Gaussian distribution function $P(g)$ embedded in many generators of random numbers. This profile corresponds to an uncorrelated roughness, $\langle g_i g_k \rangle \propto \delta_{ik}$ (white noise). What we want is to produce a surface $\mathbf{y} = y(x_i)$ with a predetermined desirable binary correlations $\zeta(x)$ (or, rather, its discrete analog ζ_{ik}),

$$\langle y_i y_k \rangle \equiv \zeta_{ik} = \int y_i y_k P[\mathbf{y}]\, d\mathbf{y}. \tag{32}$$

To achieve this, we rotate the uncorrelated vector $\mathbf{g}$ using the matrix $\widehat{A}$ [30],

$$\widehat{A} = \widehat{\zeta}^{1/2}, \quad \mathbf{y} = \widehat{A}\mathbf{g}. \tag{33}$$

This procedure allowed us to generate and analyze $1D$ and $2D$ random rough surfaces with any predetermined correlation function ζ, Eq. (32).

The computational resources required by operation (33) for large matrices $\widehat{\zeta}$ provide the only limitation on the surface size as measured in terms of step sizes $\Delta x = x_{i+1} - x_i$. This limitation is more important for $2D$ surfaces than for $1D$ ones: in addition to a size explosion in the $2D$ case, the matrices $\widehat{\zeta}$ for the $2D$ surfaces lose their almost diagonal structure even for very steep correlation functions.

The above approach cannot emulate the atomic-scale roughness with discrete amplitudes in terms of atomic sizes. In such situations, we use Monte Carlo simulations based on exactly solvable spin lattice models for which the CFs are known. The universe of the known CFs that are accessible in this way is limited by the small number of exactly solvable lattice models, mostly in $1D$. It is even unclear whether there are restrictions on the form of the CF generated in this way. What is more, in $2D$, even the simplest models, such as the Ising model, lead to the CFs for which we do not have explicit analytic expressions, making them virtually useless for our purpose. The computational limitations here are associated with long relaxation times and with the presence of large domains. We note that the experimental difficulties of extracting an accurate surface correlator also multiply when we deal with the atomic-scale roughness, even if we disregard the issue of the accuracy of profile measurements related, for example, to the tip profile [36] or the step size [37].

The simplest example of the latter approach is the ferromagnetic Ising model $y_i = \pm 1$, for which the CF is determined by the attractive coupling constant J in the Hamiltonian (or, what is the same, by the Boltzmann factors $\exp(\pm 2J/kT)$). In the $1D$ case, the CF is exponential,

$$\zeta_E(x) = \eta^2 \exp\left(-\frac{x}{r}\right), \quad r = \frac{1}{2}\exp\left(\frac{2J}{kT}\right). \tag{34}$$

Towards the end of this paper, we use this approach for designing a new rough neutron mirror for GRANIT

experiments. The CF for the $2D$ Ising model, though known in principle [38], is described by a set of complicated equations involving elliptic integrals.

We have generated numerous $1D$ and $2D$ rough surfaces using both methods: rotation of the uncorrelated surfaces with the rotation operator $\widehat{A}$ in Eq. (33) for various predetermined correlators $\widehat{\zeta}$ and Monte Carlo simulations using the Ising model. In rotations, we routinely use matrices up to 5000×5000 and in Monte Carlo simulations, up to 10^4 points x_i and 10^6 Monte Carlo cycles.

The main challenges for identifying the correlator from the data on the surface profile arise from fluctuations related to the finite size of the samples. All CFs consist of a peak at short distances and a long tail. For finite samples, the extracted correlators ζ_{ik} do not go to zero at large distances $|i-k| \gg 1$ but have long fluctuation-driven, often oscillating tails of almost constant amplitude. As a result, the standard deviation σ between the measured correlation function and the fitting function is determined by the tail area and is more or less the same for all reasonable fitting functions, which all go to zero at large distances. Meanwhile, many observables, including our $\Phi_{1,2}$, are determined by the behavior of the correlation function at small q, i. e., at large distances, and are very sensitive to the shape of the correlators. Our conclusion (see below) is that the value of σ taken by itself cannot be used for justifying the choice of the functional form of the correlation function and cannot be considered a good predictor for physical results.

Suppressing the fluctuations requires increasing the size of a sample, which, unfortunately, makes the fluctuation-driven tails longer. Another option for suppressing the fluctuation-driven tails is to average the CF over several samples, as is sometimes done in experiment [39]. This assumes that the CFs for different samples are the same and that the "true" CF does not have a long alternating tail. These assumptions can make the averaging over the samples inherently dangerous. Still, we have performed such averaging over several generated surfaces with the same true CF. Results of our numerical experiments show that if we know that there are no long-range correlations, this averaging over several samples can be helpful for $2D$ roughness, but is not necessary in $1D$. The same difficulty persists if we simply cut off the long-range tails assuming that they are driven only by the fluctuations.

Generating or measuring the CF with a large correlation radius R is virtually impossible. The important factor is not the overall number of the data points N but the number of inhomogeneities N/N_i, where N_i is the number of points in a typical inhomogeneity, which in the $2D$ case grows proportionally to R^2. The shape of the CF with not very large N/N_i is often misleading and points, rather convincingly, at fictitious long-range correlations. One should be very cautious when identifying an additional, larger correlation length from the experimental data with fat correlation tails [40].

We have also tried an alternative to the use of the fitting functions by using the spectral decomposition of the raw correlation data for direct computation of observables. In $1D$ examples, this approach has worked somewhat, but not much, better than using a fitting function of a wrong shape, although still noticeably worse than using the fitting function of the right shape. In $2D$, this approach has led to unstable results because of the fluctuation-driven anisotropy of the extracted correlators and smaller linear sizes of the samples than in $1D$.

The tables illustrate some of our results for generated rough surfaces with parameters close to those in experiments with ultracold neutrons from Sec. 3.

Table 1 shows the results of our analysis of three numerically generated $1D$ rough surfaces with the CF emulating the Gaussian correlations with $r = 1.19$ and $\eta = 0.119$. As we can see, the quality of the fits $\sigma_{G,E,PL}$ for all three types of the fitting functions is more or less the same, about $5 \cdot 10^{-4}$, but the results for the physically important parameters $\Phi_{1G,E,PL}$ differ considerably, by about 25 %. In our experiment, the "true" shape of the CF is known to be Gaussian and, not surprisingly, the fitting by the Gaussian function produces the values of Φ_1 very close to the "true" value 23.48. The inevitable conclusion is that the quality of the fit σ does not tell much about the quality of physical results obtained using this fitting function. The results for fitting by the power-law and exponential CFs were relatively close to each other and very different from those for the Gaussian fit. The explanation is simple: the Gaussian function has a much shorter tail. The use of the raw correlation data in the equations (Φ_n) works better than the use of a wrong fitting function but worse than using the right one.

The quality of the fits (the values of σ) for $2D$ roughness is worse than in the $1D$ case because of the fluctuation-driven anisotropy and smaller linear sizes of our samples, although the overall number of the data points in our numerical experiments is larger. The only noticeable difference in conclusions is that the use of raw correlation data without fitting leads to unstable results. Here, averaging over several runs leads to a marked improvement in the results for Φ_2.

Table 1. Three numerical runs for $1D$ surfaces that emulate the Gaussian correlation of inhomogeneities $\eta^2 \exp\left(-x^2/2r^2\right)$ with $r = 1.19$ and $\eta = 0.119$ (see Sec. 3)

№	r_G, $\sigma_G \cdot 10^4$	r_E, $\sigma_E \cdot 10^4$	r_{PL}, $\sigma_{PL} \cdot 10^4$	$\sigma_n \cdot 10^{17}$	Φ_{1G},	Φ_{1E},	Φ_{1PL},	Φ_{1n}
1	1.19, 5.24	1.59, 5.81	1.44, 5.81	1.92	23.86,	18.19,	18.81,	21.96
2	1.15, 4.49	1.53, 4.56	1.36, 4.64	1.83	23.33,	17.84,	18.65,	21.14
3	1.25, 4.37	1.69, 4.40	1.54, 4.47	1.69	23.56,	17.26,	17.85,	20.96

Note. The "true" value of Φ_1, Eq. (26), for such surface is $\Phi_1 = 23.48$. The extracted correlators were fitted with Gaussian $(\eta_G^2 \exp\left(-s^2/2r_G\right))$, exponential $(\eta_E^2 \exp\left(-s/r_E\right))$, and power-law $(\eta_{PL}^2/\left[1+(s/r_{PL})^2\right]^{3/2})$ fitting functions. The table contains the best fitting values of $r_{G,E,PL}$ together with $\sigma_{G,E,PL}$, and the recalculated values of $\Phi_{1G,E,PL}$. The values of $\eta_{G,E,PL}$ are very close to each other. The columns with Φ_n and σ_n give the values of Φ_1 and the standard deviation when the spectral decomposition of the raw data is put directly into equations without any fitting.

Table 2. Five Monte Carlo runs for the $1D$ Ising model

№	$r_E, \sigma_E \cdot 10^4$	$r_G, \sigma_G \cdot 10^4$	$r_{PL}, \sigma_{PL} \cdot 10^4$	$\sigma_n \cdot 10^{17}$	Φ_{1E},	Φ_{1G},	Φ_{1PL},	Φ_{1n}
1	1.27, 6.69	0.85, 6.93	1.26, 6.72	3.79	18.6,	27.4,	19.6,	25.8
2	1.23, 6.83	0.88, 6.94	1.25, 6.84	1.49	19.1,	26.8,	19.7,	26.2
3	1.04, 6.51	0.73, 6.74	1.07, 6.54	2.82	20.7,	30.2,	21.4,	27.3
4	1.18, 6.65	0.87, 6.71	1.23, 6.62	3.01	19.7,	27.1,	20.0,	26.1
5	0.94, 6.44	0.74, 6.42	1.03, 6.38	1.91	22.2,	29.8,	21.9,	27.7

Note. The "true" correlation function is exponential with $r = 1.19$, $\eta = 0.119$, and $\Phi_1 = 19.5$. The CFs extracted from the generated rough surfaces are fitted with the exponential, Gaussian, and power-law functions. The table contains the best fitting values of $r_{E,G,PL}$ and the corresponding values of $\sigma_{E,G,PL}$ and $\Phi_{1E,G,PL}$. The values of Φ_{1n} are obtained by direct spectral analysis of the raw correlation data.

Table 2 presents the results of five Monte Carlo runs for the $1D$ Ising model in application to the neutron mirror. The data in the columns are arranged similarly to Table 1. The parameters of the "true" CF are the same, $r = 1.19$ and $\eta = 0.119$. However, since the Ising model corresponds to the exponential CF, Eq. (34), and not to the Gaussian correlator as in Table 1, the true value of parameter Φ_1 in Eq. (30) is now $\Phi_1 = 19.5$. Since the simulation is based on the Ising model with spins ± 1, the extracted average amplitudes of roughness $\eta_{E,G,PL}$ differ from $\eta = 0.119$ by less than 1 % for all fitting functions. The size of the sample is $N = 1000$ and we perform 10^6 Metropolis cycles. Of course, the fit using the exponential correlator provides the best values for Φ_1. Of the other two fits, it is not clear why the power-law fit works much better than the Gaussian one. The last column in the Table 2 gives the values of Φ_{1n} obtained by direct spectral analysis with $N/2$ harmonics of the raw correlation data without any fitting. These data display the worst agreement with $\Phi_1 = 19.5$ while the value of σ_n is by 13 orders of magnitude better than σ for any of our fitting functions. The explanation is the same as before: the full set of raw data is dominated by the long correlation tails that come from the fluctuations.

The results for rough surfaces generated using the $2D$ Ising model above the phase transition do not provide any new information.

Our main conclusion is that the reliable identification of the roughness CF requires having at least some information about its shape. Without this information, the best strategy is to rely on σ only in combination with an averaging over several samples and a graphical and numerical analysis of the shape of the correlation function in the peak area.

As an application, we have analyzed the correlation properties of a rough mirror prepared for new GRANIT experiments with ultracold neutrons [41]. The rough-

ness profile has been measured in five surface areas with 2500×2500 data points in each. Even with more than $3 \cdot 10^7$ available data points, the extracted CF still has a long fluctuation-driven tail, which hinders its unambiguous identification. These fluctuation-driven tails are indistinguishable from those in our numerical experiments. The attempts to fit the extracted correlator to various fitting functions lead to noticeably different predictions for the observable Φ_2 while the statistical quality of the fits σ are more or less the same for all fitting functions. Our preferred choice, based on the averaging over five samples and the shape of the correlation peak, is the $2D$ isotropic exponential correlator with $\eta \approx 1.02$ and $r \approx 0.65$.

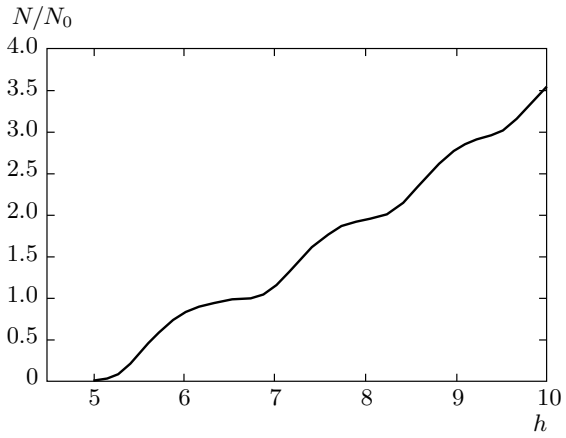

Fig. 3. The exit neutron count $N(h)/N_0$, Eq. (26), as a function of the spacing between the mirrors. Calculations for the new sapphire mirror with isotropic exponential roughness $r = 0.65$, $\eta = 1.02$

5. CONCLUSIONS

In summary, we have applied our general theory of transport of particles along rough surfaces to the gravitationally quantized neutrons in a rough waveguide. In the end, all parameters of a system collapse to a single constant $\Phi_{2,1}$ which determines the exit neutron count. The constant Φ is closely related to the depletion time (the line broadening) for the gravitational states τ_j. The required input parameters are the roughness CF and the distribution of neutrons entering the waveguide over the gravitational states. The depletion times τ_j have simple scaling properties, Eq. (31), and their ratios are the universal functions of the waveguide width (see Eq. (18) and Fig. 1).

Our numerical experiments show that the identification of the roughness CF should not be undertaken lightly. Our conclusion is that the CF must be identified by using the statistical quality of the fits σ to different fitting functions only in combination with the averaging over several experimental areas and a numerical and graphical analysis of the CF in the peak area. We do not recommend avoiding the identification of the roughness CF by inputting the raw correlation parameters directly into the equations.

Our analysis of a new neutron mirror [41] identifies the CF as the isotropic $2D$ exponential function with the correlation radius $r = R/l_0 = 0.65$ and the amplitude $\eta = \ell/l_0 = 1.02$. This fitting function yields $\Phi_2 \approx 5.22 \cdot 10^3$. The predicted neutron exit count as a function of the spacing between the rough and flat mirrors h, Eq. (26), is plotted in Fig. 3. The steps in the figure are the long-sought demonstration of consecutive depletion of the quantum gravitational states of neutrons.

The accuracy of this prediction is limited by a relatively large value of the roughness amplitude η. Any perturbative theory assumes η to be the smallest length parameter, $\eta \ll r, h$, which is clearly not true for this mirror. The same factor limits the accuracy of measuring the spacing between the mirrors and makes measurements at small h virtually impossible. This large value of η also leads to the smearing of the gravitational quantum states. Another limitation is the lack of accurate information on the distribution of neutrons over the gravitational states in front of the waveguide. We assume this distribution to be uniform at very low energies; this assumption, although reasonable, can potentially break down during the beam preparation.

In general, the sharpness of the quantum steps in the exit neutron count $N_e(h)$ is determined by the difference in values between $\exp(-t_L/\tau_j)$ with different j, which is determined by the values of $1/\tau_j$ in Fig. 2 adjusted by the scaling relation (31). Since the distance between the starting points for the state depletion in Fig. 2 is not large, the best way to see these quantum steps is to increase the time of flight t_L.

Most of the uncertainties disappear if a future rough mirror is designed differently. Our recommendation is to use $1D$ roughness based on the Monte Carlo simulations for the $1D$ Ising model (the grating of constant amplitude but with random width and separation of trenches, Fig. 4). The preferred correlation radius is $r \approx 2$ with the amplitude of roughness in the 0.2–0.4 range. Since all the lengths are in the units of 5.87 μm, the transfer of the generated profile onto a real surface

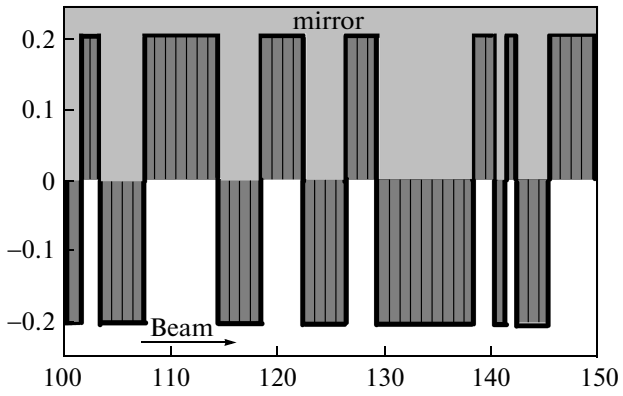

Fig. 4. A fragment of the rough upper mirror based on Monte Carlo simulations for the $1D$ Ising model (the Ising mirror). The thick black line is the surface profile and dark bars are "Ising spins". Mirror material (sapphire) is above the thick black line (all dark and light filled areas). The amplitude of roughness is $\eta = 0.2$, the correlation radius is $r = 2$, and $\Phi_1 \approx 43.5$. Both axes are in units of $l_0 = \hbar^{2/3}\left(2m^2g\right)^{-1/3} \approx 5.871\ \mu$m and the vertical scale is about 100 times smaller than the horizontal one. Changing the value of η can be done simply by rescaling the vertical axis

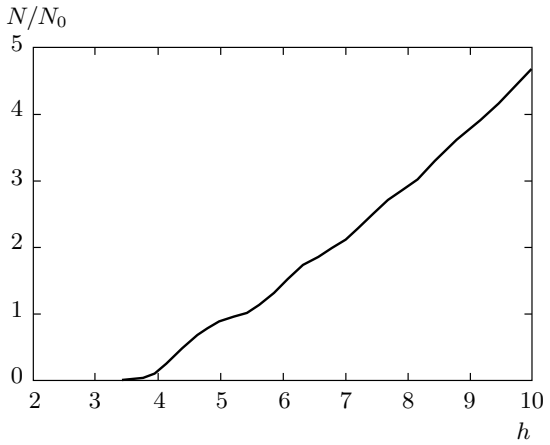

Fig. 5. The exit neutron count $N(h)/N_0$, Eq. (26), for the Ising mirror similar to the one in Fig. 2. The roughness amplitude is $\eta = 0.4$ and the correlation radius is $r = 2$. The steps can be made more pronounced by increasing η

seems to be technologically feasible. The thick black line in Fig. 4 shows the mirror profile and the grey bars are the up and down "Ising spins". We note that the vertical scale is about 100 time smaller than the horizontal one and the roughness is very mild.

The correlation function $\zeta(x)$ for the continuous "Ising mirror" such as in Fig. 4 is close to the exponential one for the discrete $1D$ Ising model, Eq. (34), and coincides with it at the integer points of x,

$$\zeta(x) = \eta^2 \left[\exp\left(-\lfloor x\rfloor/r\right) + (x - \lfloor x\rfloor) \times \right.$$

$$\left. \times \left(\exp\left(-\lceil x\rceil/r\right) - \exp\left(-\lfloor x\rfloor/r\right)\right)\right]. \quad (35)$$

The values of Φ_1 for the true Ising correlator $\zeta(x) = \eta^2 \exp(-x/r)$ are given by Eq. (30) and yield Φ_1 for $r = 2$ and $\eta = 0.2$–0.4 in the 42.5–170 range with $t_L/\tau_0 \approx 23$ (the old cell) and in the 30.3–121.5 range for $t_L/\tau_0 \approx 26$ (the new cell). Although we cannot give a simple analytic expression for Φ_1 for correlation function (35), the numerical results for this correlator differ from the ones for the pure Ising exponent at $r = 2$ by about (3–5) %. These values of Φ_1 are sufficient for exhibiting the quantum steps in the exit neutron count (Fig. 5) and for producing neutrons with well-defined energies in the peV range.

The experimental advantage of this design is the perfectly controllable $1D$ environment with the preservation of the quantum states and without the spikes on the surface. It allows accurate measurement of the spacing between the mirrors and minimizes the loss of neutrons due to the sideway scattering.

One of the authors (A. M.) appreciates the invitation to participate in this special issue of JETP honoring the 75th birthday of his Ph. D. advisor in the mid-1970s, A. F. Andreev, and remembers with gratitude years of joint work. We acknowledge productive discussions with P. Nightingale (URI) on certain computational aspects of the work and a long history of constructive exchanges with V. Nesvizhevsky (ILL) and other members of the GRANIT collaboration. Some of the results have been presented at GRANIT-2014 Workshop (Les Houches, France, March 1–7, 2014) [41, 42].

REFERENCES

1. F. G. Bass, and I. M. Fuks, *Wave Scattering from Statistically Rough Surfaces*, Pergamon, New York (1979).

2. J. A. DeSanto and D. S. Brown, *Analytical Techniques for Multiple Scattering from Rough Surfaces*, Progress in Optics, Vol. 23, ed. by E. Wolf, North-Holland, Amsterdam (1986).

3. J. A. Ogilvy, *Theory of Wave Scattering from Random Surfaces*, Adam Hilger, Bristol (1991).

4. A. G. Voronovich, *Wave Scattering at Rough Surfaces*, Springer, Berlin (1994).

5. A. E. Meyerovich and A. Stepaniants, Phys. Rev. B **60**, 9129 (1999).

6. G. Fishman and D. Calecki, Phys. Rev. Lett. **62**, 1302 (1989); Phys. Rev. B **43**, 11581 (1991).

7. Z. Tesanovic, M. V. Jaric, and S. Maekawa, Phys. Rev. Lett. **57**, 2760 (1986).

8. N. Trivedi and N. W. Ashcroft, Phys. Rev. B **38**, 12298 (1988).

9. A. E. Meyerovich and S. Stepaniants, Phys. Rev. Lett. **73**, 316 (1994); Phys. Rev. B **51**, 17116 (1995).

10. A. E. Meyerovich and A. Stepaniants, Phys. Rev. B **58**, 13242 (1998).

11. A. Stepaniants, D. Sarkisov, and A. Meyerovich, J. Low Temp. Phys. **114**, 371 (1999).

12. A. E. Meyerovich and A. Stepaniants, J. Phys.: Cond. Matt. **12**, 5575 (2000); S. Chatterjee and A. E. Meyerovich, Phys. Rev. B **81**, 245409 (2010); *ibid*, **84**, 165432 (2011).

13. A. E. Meyerovich and D. Chen, Phys. Rev. B **66**, 235306 (2002).

14. I. B. Altfeder, D. M. Chen, and K. A. Matveev, Phys. Rev. Lett. **80**, 4895 (1998).

15. YiYing Cheng and A. E. Meyerovich, Phys. Rev. B **73**, 85404 (2006).

16. A. E. Meyerovich and I. V. Ponomarev, Phys. Rev. B **65**, 155413 (2002).

17. V. V. Nesvizhevsky et al., Nature **415**, 297 (2002); V. V. Nesvizhevsky et al., Phys. Rev. D **67**, 102002 (2003); V. V. Nesvizhevsky et al., Europ. Phys. J. C **40**, 479 (2005).

18. V. I. Luschikov and A. I. Frank, JETP Lett. **28**, 559 (1978).

19. V. V. Nesvizhevsky and K. V. Protasov, in *Trends in Quantum Gravity Research*, ed. by D. C. More, Nova Sci. Publ. (2006), p. 65; V. V. Nesvizhevsky, Physics–Uspekhi **53**, 645 (2010).

20. T. Jenke, P. Geltenbort, H. Lemmel, and H. Abele, Nat. Phys. **7**, 468 (2011); L. A. Chizhova, S. Rotter, T. Jenke, G. Cronenberg, P. Geltenbort, G. Wautischer, H. Filter, H. Abele, and J. Burgdörfer, Phys. Rev. E. **89**, 032907 (2014).

21. G. Ichikawa, S. Komamiya, Y. Kamiya, Y. Minami, M. Tani, P. Geltenbort, K. Yamamura, M. Nagano, T. Sanuki, S. Kawasaki, M. Hino, and M. Kitaguchi, Phys. Rev. Lett. **112**, 071101 (2014).

22. Ya. B. Zeldovich, JETP **9**, 1389 (1959); V. I. Lushchikov, Yu. N. Pokotilovskii, A. V. Strelkov, and F. L. Shapiro, JETP Lett. **9**, 23 (1969); V. K. Ignatovich, *The Physics of Ultracold Neutrons*, Clarendon, Oxford (1990); R. Golub, D. J. Richardson, and S. K. Lammoreux, *Ultracold Neutrons*, Higler, Bristol (1991).

23. G. Breit, Phys. Rev. **32**, 273 (1928).

24. J. H. Freed, Ann. Phys. Fr. **10**, 901 (1985).

25. H. Murayama, G. G. Raffelt, C. Hagmann, K. van Bibber, and L. J. Rosenberg, in K. Hagiwara et al. (Particle Data Group), *Review of Particle Properties*, p. 374; Phys. Rev. D **66**, 010001 (2002).

26. V. V. Nesvizhevsky and K. V. Protasov, Class. Quant. Gravity, **21**, 4557 (2004).

27. V. V. Nesvizhevsky et al., Nucl. Instr. Meth. A **578**, 435 (2007).

28. A. E. Meyerovich and V. V. Nesvizhevsky, Phys. Rev. A **73**, 063616 (2006).

29. R. Adhikari, Y. Cheng, A. E. Meyerovich, and V. V. Nesvizhevsky, Phys. Rev. A **75**, 063613 (2007).

30. M. Escobar and A. E. Meyerovich, Phys. Rev. A **83**, 033618 (2011).

31. A. Yu. Voronin, H. Abele, S. Baessler, V. V. Nesvizhevsky, A. K. Petukhov, K. V. Protasov, and A. Westphal, Phys. Rev. D **73**, 044029 (2006); A. Voronin, Compt. Rend. Phys. **12**, 724 (2011).

32. V. V. Nesvizhevsky, private communication.

33. J. A. Ogilvy and J. R. Foster, J. Phys. D: Appl. Phys. **22**, 1243 (1989).

34. A. Fubel, M. Zech, P. Leiderer, J. Klier, and V. Shikin, Surf. Sci. **601**, 1684 (2007).

35. M. Escobar and A. E. Meyerovich, arXiv:1404.1291v2 [cond-mat.dis-nn].

36. *Scanning Tunneling Microscopy*, ed. by J. A. Stroscio and W. J. Kaiser, Acad. Press, New York (1993), Methods of Experimental Physics, Vol. 27.

37. R. C. Munoz, G. Vidal, M. Mulsow, J. G. Lisoni, C. Arenas, A. Concha, F. Mora, R. Espejo, G. Kremer, L. Moraga, R. Esparza, and P. Haberle, Phys. Rev. B **62**, 4686 (2000).

38. J. D. Johnson, S. Krinsky, and B. M. McCoy, Phys. Rev. A **8**, 2526 (1973); Hung Cheng and Tai Tsun Wu, Phys. Rev. **164**, 719 (1967).

39. M. E. Robles, C. A. Gonzalez-Fuentes, R. Henriquez, G. Kremer, L. Moraga, S. Oyarzun, M. A. Suarez, M. Flores, and R. C. Munoz, Appl. Surf. Sci. **258**, 3393 (2012).

40. P. Sharma, A. Córcoles, R. G. Bennett, J. M. Parpia, B. Cowan, A. Casey, and J. Saunders, Phys. Rev. Lett. **107**, 196805 (2011).

41. M. Escobar, F. Lamy, A. E. Meyerovich, and V. V. Nesvizhevsky, Adv. High Energy Phys. **2014**, 76418 (2014).

42. M. Escobar and A. E. Meyerovich, Adv. High Energy Phys. **2014**, 185414 (2014).